THE JOURNAL OF PHYSICAL CHEMISTRY C

Article

pubs.acs.org/JPCC

Infrared Spectroscopic Studies of Conduction Band and Trapped Electrons in UV-Photoexcited, H-Atom n-Doped, and Thermally Reduced TiO_2

Dimitar A. Panayotov, Steven P. Burrows, and John R. Morris*

Department of Chemistry, Virginia Tech, Blacksburg, Virginia 24061-0212, United States

Supporting Information

ABSTRACT: Transmission FTIR spectroscopy is used to explore the electronic structure of excited TiO_2 nanoparticles. Broad infrared spectral features in UV-photoexcited, n-doped, and thermally reduced titania are found to be well-described by two theoretical models, which independently account for the creation of free conduction band electrons and trapped localized electrons that occupy states within the band gap. The infrared spectra indicate that the trapped electrons reside at shallow donor levels that exist 0.12−0.3 eV below the conduction band minimum. IR excitation of the trapped electrons is evidenced by a broad feature in the spectra, which exhibits a maximum that corresponds to the energy of the donor level. These features are well described by a hydrogenic-effective mass model. In addition, free conduction band electrons have a dramatic effect on the infrared spectra by exhibiting a broad featureless absorbance that increases exponentially across the entire mid-IR range. This absorbance is the result of intraconduction band transitions, for which free electron coupling to acoustic phonons is required to conserve momentum. Both localized (within the band gap) and delocalized (within the conduction band) electrons are found to exist in TiO_2 when excess electrons (are created by different means: UV photoexcitation in the presence of a hole scavenger (methanol), irradiation with atomic hydrogen, and thermal removal of lattice oxygen.

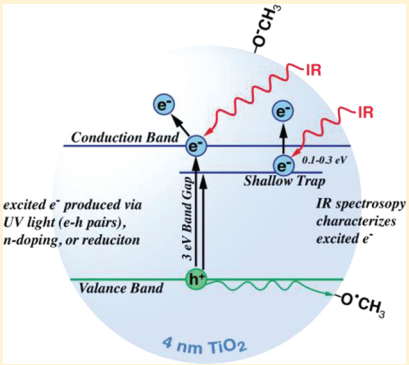

1. INTRODUCTION

Titanium dioxide is a wide-band-gap semiconductor that has been utilized as the active material in a range of applications including heterogeneous catalysis, coating and sensor development,[1,2] photodegradation of hazardous pollutants,[3−6] and conversion of solar energy.[7] Spurred by the large number of practical applications, fundamental research into the photochemistry and chemistry of single-crystal and nanoparticulate TiO_2 has grown tremendously. However, there have been surprisingly few studies into the energetics of electronic states within TiO_2 that play a critical role in the surface chemistry of this material. In addition, recent reviews, one by Yates et al.[8] and one by Henderson,[9] highlight the need for fundamental research that can bridge a gap in the understanding of electronic states for well-defined single-crystal TiO_2 with those states found in more practical polycrystalline TiO_2, such as nanoparticles. Therefore, we have worked to characterize the populations of both shallow-trapped (ST) electrons and free conduction band (CB) electrons that are created during three independent means of producing excited electronic states in titania nanoparticles. By developing a model for characterizing ST and CB electronic populations using infrared spectroscopy, these studies demonstrate that many of the same concepts for describing charge carrier behavior in single-crystal systems also apply to small, polymorphous nanoparticulate systems.

One of the many interesting properties of TiO_2 is the readiness by which both polymorphs (anatase and rutile) of this oxide lose lattice oxygen.[10] Surface and bulk oxygen deficiencies, characterized as Ti^{3+} ions,[6,11,12] can be created by a variety of chemical and physical processes. These crystal defect sites govern many of the unique properties of the material and are of fundamental importance for a number of applications.[1,5,6,12] The two excess electrons that are created for each oxygen vacancy are associated with intrinsic donor defects where they fill new electronic states that exist ∼1 eV below the conduction band minimum (CBM).[1,2] Many spectroscopic signatures of the Ti^{3+} ions in reduced TiO_2 have been identified through a variety of techniques, such as: (i) near-infrared (IR) absorption at energies of ∼1 eV;[13] (ii) a broad spectroscopic signature at ∼0.9 eV below the Fermi level (E_F)[2,14−18] has been observed via ultraviolet photoelectron spectroscopy and electron energy loss spectroscopy;[11,19−21] (iii) electron paramagnetic resonance has shown evidence for multiple types of Ti^{3+} ions in the TiO_2 lattice;[22−24] and (iv) absorption spectroscopic studies in the visible range have shown evidence for bands assigned to d−d type transitions.[25] Interestingly, the energy of these trap levels and the likely localization of the electronic charge at Ti^{3+} sites suggest they behave as deep donors, which is contrary to the expected energetics that likely govern the well-established n-type conductivity of reduced

Received: June 6, 2011
Revised: November 23, 2011
Published: January 10, 2012

   dx.doi.org/10.1021/jp2053103 | J. Phys. Chem. C 2012, 116, 4535−4544

TiO_2.[26,27] However, the work by Ghosh et al.[28] has, in fact, reported at least eight electron trap levels that exist at energies from only 0.27 to 0.87 eV below the conduction band edge for single crystal rutile. Their work was among the first to propose that different types of Ti^{3+} species can exist within the same sample. Today, interband states with ionization energies near 1 eV are referred to as "shallow levels" while levels with ionization energies greater than 1.5 eV are termed "deep levels".[28] As suggested by Di Valentin et al., the main differences between many of these spectroscopic approaches for studying titania may be that particular methods mainly probe bulklike Ti^{3+} ions, while others are more sensitive to ions at the surface.[29] Fujimori et al.[30] were among the first to propose a model that explains the discrepancy between the large energy (~1 eV) observed in the photoemission spectra and the small energy (~0.1 eV) measured for transport properties. Their model is based on simultaneous short-range (Holstein-type) and long-range (Frölich-type) interactions between charge carriers and the ionic lattice.[30]

Recently, increasing research effort has been devoted to unraveling the nature of the band gap states (BGS) in reduced TiO_2.[17,18,31−40] Numerous studies have shown evidence that oxygen vacancies (O_{vac}) are the origin of the BGS in TiO_2.[1,18,39,41] Alternatively, other studies suggest that Ti interstitial defect sites (Ti_{int}) play the major role in defining the BGS and have a more significant influence on the chemistry of titania.[17,33,36,42,43] Furthermore, the spatial distribution of the excess charge (or extent of delocalization) related to O_{vac} sites, Ti_{int} sites, and H dopants is not well understood, and extensive experimental and theoretical research into this problem continues to progress.[29,31−34,36,37,44−50]

Unfortunately, detailed theoretical descriptions of the electronic structure of defects in titania remains a challenge because of the strongly correlated nature of d-electrons in TiO_2. For example, pure density-functional theory (DFT) calculations indicate that the states associated with defects are completely delocalized and the corresponding density of states is void of band gap states, which is inconsistent with the large body of experimental evidence.[44] The two most common approaches for treating electron correlation in these systems are the hybrid functionals[31,37,44,45] (a mix of DFT and Hartree−Fock) and the so-called DFT+U method (added Hubbard-U term).[29,31,38,50,51] Through employing the hybrid functional approach, Janotti et al. have suggested that the O_{vac} sites are shallow donors for which the +2 charge state is lower in energy than both the neutral and the +1 state for all Fermi-level positions in the band gap.[37] Di Valentin et al. have employed both DFT+U and hybrid functional approaches to explore the nature of Ti^{3+} species produced by reduction and n-type doping of TiO_2.[29] They found evidence for highly localized excess electrons at a single Ti^{3+} site along with some delocalized solutions where the extra charge is distributed over several Ti ions. Stausholm-Møller et al.[50] used the DFT+U method to find that Ti_{int} sites, O_{vac} sites, and H dopants create gap states that have very similar mean energies about 0.94 eV below the CBM. Kowalski et al.[45] further explored the distribution of charge within titania, which led them to propose that excess electrons preferentially populate the second subsurface layer but that they are not confined and there is some probability of also finding electrons at surface sites and at other subsurface layers. Mattioli et al. have shown that, in anatase, an oxygen vacancy can induce a shallow electronic level that is high in energy and strongly delocalized, together with a deep and localized level.[48] In contrast, the same defect appears to induce only deep localized levels in rutile.[48] Most recently, two different research groups, Chiodo et al.[52] and Kang et al.,[53] have shown that a combination of density-functional theory and many-body perturbation-theory techniques produces a high-quality description of electronic and optical properties of TiO_2 in both its anatase and rutile forms. These approaches show that the optical excitations are strongly anisotropic with significant excitonic localization within the anatase phase.[52] Overall, the theoretical studies suggest that O_{vac} and Ti_{int} defects behave as deep donors prior to significant structural changes in the lattice, but subsequent structural relaxations create shallow donors. Minato et al. have further extended our understanding of the difference between the instantaneous and relaxed density of states (DOS) and showed, by both experimental and theoretical approaches, that the excess charge at O_{vac} sites is delocalized over multiple surrounding titanium atoms.[34] Therefore, one may speculate that deep donor levels should be observed experimentally by methods that probe instantaneous vertical excitations, while the thermodynamically favored shallow donor states may be detected by alternate approaches.[38]

The experimental work described below complements these previous studies by characterizing the electronic structure of shallow donor states in particulate titania created through ultraviolet excitation or n-doping. Furthermore, this work probes the nature of the conduction band electrons that are often created in concert with any electronic excitation in TiO_2. Perhaps most importantly, this work demonstrates that both free conduction band electrons (CBEs) and shallow trapped electrons (STEs) in TiO_2 nanoparticles can be detected by transmission Fourier-transform infrared (FTIR) spectroscopy. The free CBEs exhibit the typical exponential frequency dependent spectrum that is attributed to indirect intra-CB optical transitions. In contrast, the spectral signature for the STEs is characterized by a broad absorption in the mid-IR region that is accurately described by a direct optical transition from a hydrogenic-like donor center into the conduction band. Finally, the data from this work show that the STEs can be created in small 4 nm rutile particles as well as larger 25 nm mixed-phase titania.

2. EXPERIMENTAL SECTION

The small 4 nm rutile nanoparticles employed in this study were prepared by laser vaporization of bulk TiO_2 in an O_2 atmosphere according to previously described procedures.[54] The larger particles, obtained commercially (Degussa P25), were created by the Aerosil process (i.e., via flame hydrolysis).[55] P25 particles are composed of 80% anatase with average size of 25 nm and 20% rutile nanoparticles of 33 nm average diameter.[56] A third sample consisting of TiO_2-supported Au particles was developed for exploring the H_2-dissociative adsorption and subsequent H atom n-doping of the titania. The Au/TiO_2 sample was prepared by the deposition−precipitation method.[57] Transmission electron microscopy (TEM) of the Au/TiO_2 particles showed the average diameter of the deposited gold nanoparticles to be 2.7 nm. Inductively coupled plasma spectroscopic analysis indicated that the Au/TiO_2 particles used in this study contained 8% w/w gold loading. TEM images and X-ray diffraction patterns of each TiO_2 material are presented in Figure S1 of the Supporting Information.

dx.doi.org/10.1021/jp2053103 | J. Phys. Chem. C 2012, 116, 4535−4544

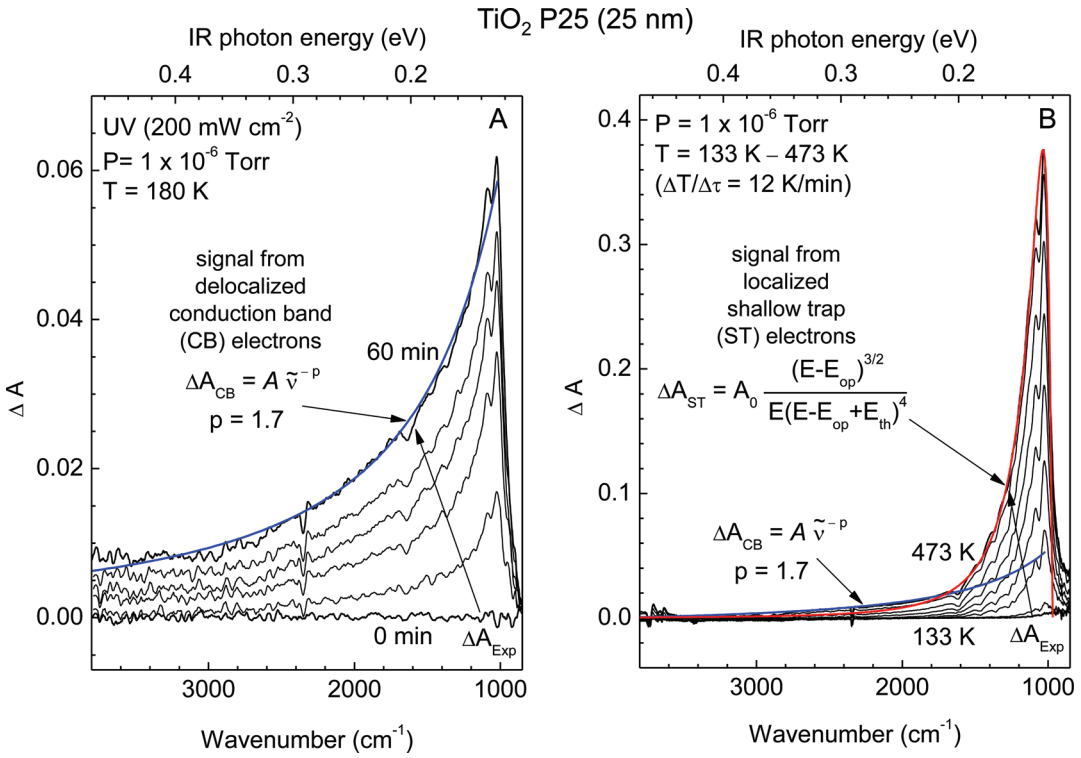

Figure 1. Infrared spectra of clean, 25 nm particles of P25 TiO_2 recorded during: Panel A: 60 min UV irradiation by 3−5 eV (200 mW cm^{-2}) photons in vacuum at 180 K, and Panel B: thermal annealing in vacuum from 133 to 473 K at a heating rate of 12 K min^{-1}. The smooth red line in panel B is the model for the IR absorbance of STEs and the blue line in both figures represents a model for the IR absorbance due to CBE transitions.

For the IR spectral measurements, the TiO_2 sample was held as a pressed powder on a tungsten grid with 80% transmission. The high vacuum (1×10^{-8} Torr) IR cell and the all-metal vacuum system have been described in detail elsewhere.[57−59] Transmission IR spectra were acquired at 4 cm^{-1} spectral resolution by a liquid-nitrogen cooled Hg/Cd/Te IR detector on an N_2-purged Mattson Research Series I FTIR spectrometer. A 350 W Hg arc (Oriel Corp.) UV lamp was used as the photon source in the photoexcitation experiments.[23] Finally, for atomic doping experiments, gas-phase hydrogen atoms were produced in the main vacuum chamber using a coiled tungsten filament maintained at 1800 K during exposure to a continuous flow of molecular hydrogen at 0.20 Torr pressure.[58] Thermal radiation from the hot filament was shielded from the titania samples by a stainless steel baffle. Water vapor impurities were reduced significantly by maintaining a reentrant Dewar in the IR cell at 77 K during all experiments.

The TiO_2 samples, typically weighing 6−7 mg/cm^2, were activated in vacuum at 673 K for 4 h and then treated with 20 Torr of O_2 for 60 min at the same temperature. This annealing temperature (673 K) is far below the temperatures reported previously for nucleation controlled transformation of nanocrystalline anatase to rutile, which occurs above 850 K.[60] This procedure removes the adsorbed water and traces of residual organic species.[61] After evacuation at 673 K, oxygen was readmitted for 30 min; then the samples were cooled to 473 K, evacuated to 1×10^{-6} Torr, and cooled to room temperature. In the following sections, the thermally annealed TiO_2 samples are referred to as the clean particles.[54,58] Prior to use, the Au/TiO_2 sample was activated by an analogous procedure, but the temperature was limited to 473 K to avoid thermal-activated diffusion and subsequent aggregation of Au nanoparticles.[57]

3. RESULTS AND DISCUSSION

As described in the Introduction, previous studies have shown that optical absorption of radiation by electrons and holes in TiO_2 occurs over a very broad spectral region, ranging from the UV to the IR.[62−66] In fact, infrared spectroscopy has been employed in many studies of delocalized electrons in TiO_2 materials.[23,58,62,66−72] In addition to direct spectroscopic probes, hole- and electron-scavenging molecules have been used to investigate the energetics of trapped charges created during UV-light irradiation.[62−66] In the present work, we employed three alternate routes to create excess electrons (defects) in TiO_2: (1) UV excitation in the presence of a hole scavenger (methanol), (2) active n-doping of the TiO_2 via irradiation with atomic hydrogen, and (3) thermal annealing to remove lattice oxygen. For each approach, we find that transmission infrared spectroscopy is an effective probe of the resulting electronic structure for this wide-band-gap semiconductor.

3.1. Free CB Electrons in UV-Photoexcited Clean TiO_2 Nanoparticles. The infrared spectra shown in black in Figure 1A were recorded at 180 K for the clean, 25 nm particles of P25 TiO_2 during UV irradiation by 3−5 eV (200 mW/cm^{-2}) photons. The monotonic IR absorption that starts at ∼4000 cm^{-1} and increases exponentially toward 1000 cm^{-1} (where the spectral cutoff, due to bulk Ti−O skeletal vibrations, appears in titania[73]) is attributed to IR absorption by the UV-generated free CBEs.[23,64,68,70,74,75] Free CB electrons that are involved in *k*-nonconserving indirect optical transitions, of the type observed in these studies, are assisted by TiO_2 lattice phonon modes or other scattering centers to conserve momentum.[76−78] Such IR absorption can be characterized by a simple model based on classical electromagnetic theory, taking into account

dx.doi.org/10.1021/jp2053103 | J. Phys. Chem. C 2012, 116, 4535−4544

the effective masses of electrons and holes.[76−78] This model shows that absorption of light due to free carriers in the mid-IR region varies as

$$\Delta(\text{absorbance}) = A\nu^{-p} \quad (1)$$

where A is a scaling parameter, ν is the wavenumber of the IR light, and the exponent, p, is a characteristic of the scattering mechanism. That is, values for p = 1.5, 2.5, and 3−3.5 are predicted for acoustic-mode scattering, optic-mode scattering, and ionized-impurity scattering, respectively.[76−78] IR absorption due to delocalized electrons that exhibit scattering constants in the range of 1.5−1.7, as observed here (see the theoretical spectrum, shown in blue, in Figure 1A), is due to scattering processes involving acoustic phonons, as previously reported for UV-excited TiO_2 nanoparticles.[23,62,64,66,79,80] Therefore, the origin of the broad featureless absorbance in Figure 1A is attributed to the IR excitation of free CBEs mediated through acoustic phonon-coupled scattering.[23,62,64,66−70,75,79,80]

3.2. Shallow-Trap Electrons in Thermally Excited TiO_2 Nanoparticles. In addition to characterizing the UV-excited conduction band electrons in titania, we find that infrared spectroscopy can probe thermally populated shallow-trap states that exist below the conduction band. The infrared spectra shown in black in Figure 1B were obtained with the clean, 25 nm, TiO_2 during thermal excitation in vacuum from 133 to 473 K at a heating rate of 12 K/min. The IR spectra were recorded in 10 K intervals. The intense IR peak at ∼1100 cm^{-1} that emerges during heating was found to be completely reversible and diminished to baseline upon cooling the sample. This reversible behavior with thermal energy suggests the electronic origin of this band. However, the poor fit of eq 1 to the data (i.e., by the $\Delta A \sim \nu^{-p}$ dependence for CBEs, the blue line in Figure 1B) shows that thermal energy in this range was insufficient to directly populate the conduction band. Rather, we hypothesize that this IR spectral feature is related to direct electronic transitions involving discrete states that are located at energies below the conduction band,[28,78] i.e., electrons trapped at shallow donor levels that lead to the effective n-type conductivity of TiO_2.

The prediction that an electron in an ionic crystal could be trapped by self-induced lattice polarization and deformation was first predicted by Landau[81] and further discussed in detail by Mott and Gurney.[82] Energetically, this type of electron trap state is now known to reside within the band gap of semiconducting particles, and assuming a Coulombic potential, the energetics may be described by a hydrogenic model: that is, a mobile point charge confined to an orbit around the trap center.[78,83−86] Within this model, the optical process responsible for infrared absorption is due to an electronic transition from the 1s state associated with the "hydrogenic donor center" into the conduction band.[85,87] Assuming the presence of one electron at the bottom of the conduction band, the hydrogenic ionization energy of the 1s electron is given by[86,88]

$$E = \frac{e^4 m^*}{2\hbar\varepsilon^2} \quad (2)$$

where m^* is the isotropic effective mass of the bound electron and ε is the static dielectric constant of the crystal. Typical applications of this mode set $\varepsilon = \varepsilon_\infty$, where ε_∞ is the high-frequency dielectric constant.[86]

The optical transitions for shallow trapped electrons in semiconductors have been previously described by the theory of Koda and co-workers for Al-doped ZnS.[85,87] Their model is based on eq 2 with an effective dielectric constant, ε^* (calculated from ε and ε_∞ according to ref 89), to account for the effect of the ionic polarization of the lattice around the donor center due to the motion of the bound electron. In polar crystals, this effect leads to optical ionization energies that are necessarily larger than thermal energies.[85] That is, when an electron is bound at a donor center, polarized lattice ions become displaced to new equilibrium positions, which define a new total energy for the system, referred to as E_d for the following discussion. According to Franck−Condon type transitions,[38,78] at the instant when the bound electron is removed from the donor center, the ground-state polarization remains momentarily constant and the ions momentarily maintain their positions. The total energy of this new instantaneous configuration is referred to as E_c'. The polarization then relaxes (Franck−Condon shift[38]) as the ions respond to the new potential energy gradient and relocate to new equilibrium positions, which defines a final total energy, E_c, which is necessarily smaller than E_c'. Thus, the optical (or vertical) ionization energy of the bound electron is given by $E_{op} = E_c' - E_d$ and the thermal energy by $E_{th} = E_c - E_d$. As was previously discussed[28,30,86,89] and recently shown theoretically,[38,49] the difference between vertical and thermodynamic transition levels is closely related to the polaron-like nature of the donor-defect[86] electronic state. A more complete description of the difference between thermal (E_{th}) and optical (E_{op}) ionization energies for an oxygen vacancy is provided in the recent work by Mattioli et al.[38]

Accurately modeling the IR spectrum of the STEs requires a model that describes transitions from a bound state into the CB continuum. For this purpose, Koda et al. employed a theoretical approach based on the effective mass approximation and k-p perturbation, which yields the expression[85,87]

$$K = K_0 \frac{(E - E_{op})^{3/2}}{E(E - E_{op} + E_{th})^4} \quad (3)$$

where K_0 is the absorption coefficient, E represents the IR photon energy, E_{op} is the optical depth (the minimum photon energy required for the release of an electron from a trap), and E_{th} is the thermal depth (the energy for excitation of an electron by thermal energy) of the 1s electron in the donor center. The red line in Figure 1B shows that the experimental IR spectrum is described exceptionally well by eq 3 with E_{op} = 0.12 eV and E_{th} = 0.015 eV.

The excellent fit of the experimental data to the model for describing IR absorption by STEs suggests that there is a negligible number of free charge carriers (n) and a large number of ionized donors (D^+) for this nanoparticulate semiconductor; i.e., in clean TiO_2 nanoparticles, $n \ll D^+$. Such behavior is indicative of strong compensation by acceptor centers, a characteristic of n-type oxides.[78] In these systems, the Fermi level is pinned close to the donor level at donor ionization energies below the conduction-band edge. Therefore, we have applied an Arrhenius analysis to the thermal excitation data of Figure 1B to determine the activation energy for carrier production, which is the donor ionization energy (E_{DI}). The observed rise in the integrated ΔA_{Exp} with temperature, which is proportional to the number of produced carriers, is shown in Figure 2. The inset in Figure 2 presents an

dx.doi.org/10.1021/jp2053103 | J. Phys. Chem. C 2012, 116, 4535−4544

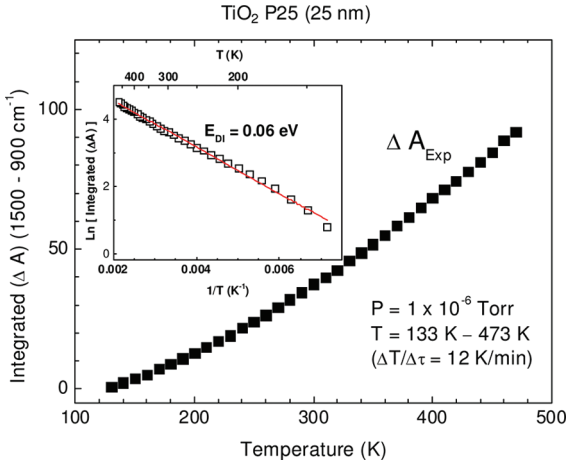

Figure 2. Rise in the integrated IR electronic absorbance, ΔA_{Exp}, as observed in Figure 1B, which is proportional to the number of carriers produced during thermal excitation. Inset: Arrhenius plot of the IR data, where the donor ionization energy, E_{DI}, is determined from the slope of the plot according to the relationship, $\ln[\Delta A] = E_{DI}/T$.

Arrhenius plot of the IR data, where the donor ionization energy, E_{DI}, is determined from the slope of the plot according to the relationship, $\ln[\Delta A] = E_{DI}/T$.

The trends shown in Figures 1 B and 2 are likely due to thermally activated electron hopping from one localized state to another, as previously described for charge carriers in crystalline and noncrystalline materials.[86,88] The experimentally determined energy for the thermally activated ionization of a donor state, E_{DI} = 0.06 eV, is very small but agrees well with the calculations by Bogomolov et al.[89] (see also refs 79 and 80), which report activation energies of 0.07 eV for conduction along the *c*-axis of the crystal and up to 0.13 eV for electron motion perpendicular to this axis.

3.3. Free CB and ST Electrons in UV-Excited TiO_2 Precovered with a Hole Scavenger. Notably absent from the IR spectrum for the UV-irradiated clean particles in Figure 1A are any features due to electronic transitions involving the discrete states that are located at energies slightly below the conduction band.[64] While most likely populated by the broad-band UV source, we hypothesize that these shallow trapped electrons recombined extremely rapidly with holes to preclude any contribution to the overall IR spectrum. We have tested this hypothesis by preadsorbing a layer of methanol, an excellent hole scavenger,[22,65,90,91] prior to UV irradiation. The spectra in Figure 3A show the time evolution of the methanol-covered surface during UV exposure. This series of spectra demonstrates that both, the exponential feature due to CBE transitions (shown by the dashed lines in blue) and a broad peak with a clear maximum at ~1800 cm^{-1} that resides on top of the exponential signal of CBEs, increase steadily with UV exposure. The character of this new spectral feature is not consistent with vibrational excitation of the adsorbate, which should result in relatively narrow bands in the higher and lower wavenumber regions of the spectrum. Furthermore, the intensity of the broad signal is related directly to the duration of UV irradiation for constant methanol coverage, which

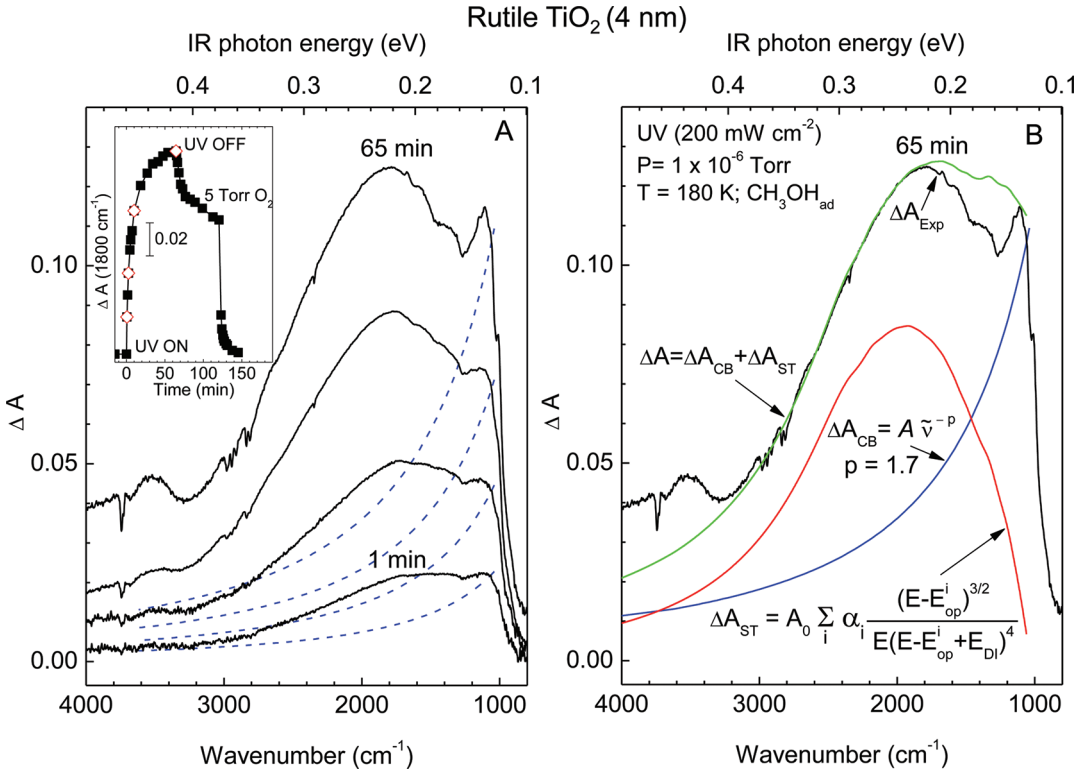

Figure 3. Infrared spectra of methanol-covered 4 nm rutile TiO_2 particles recorded during UV irradiation by 3–5 eV (200 mW cm^{-2}) photons in vacuum at 180 K. Panel A: time evolution of TiO_2 spectra during UV exposure. Inset in panel A: time dependence to the IR absorbance at 1800 cm^{-1} during and after UV exposure at 180 K, and Panel B: the composite effects of absorption by free conduction band (CB) electrons and shallow trap (ST) electrons appeared as two broad, but distinct, spectral features. As in Figure 1, the red trace is a model for the spectral response for shallow-trapped electrons and the blue line is the model for the IR spectrum of the free conduction band electrons. The direct sum of these two models is shown in green (see the text for details and fitting parameters).

dx.doi.org/10.1021/jp2053103 | J. Phys. Chem. C 2012, 116, 4535–4544

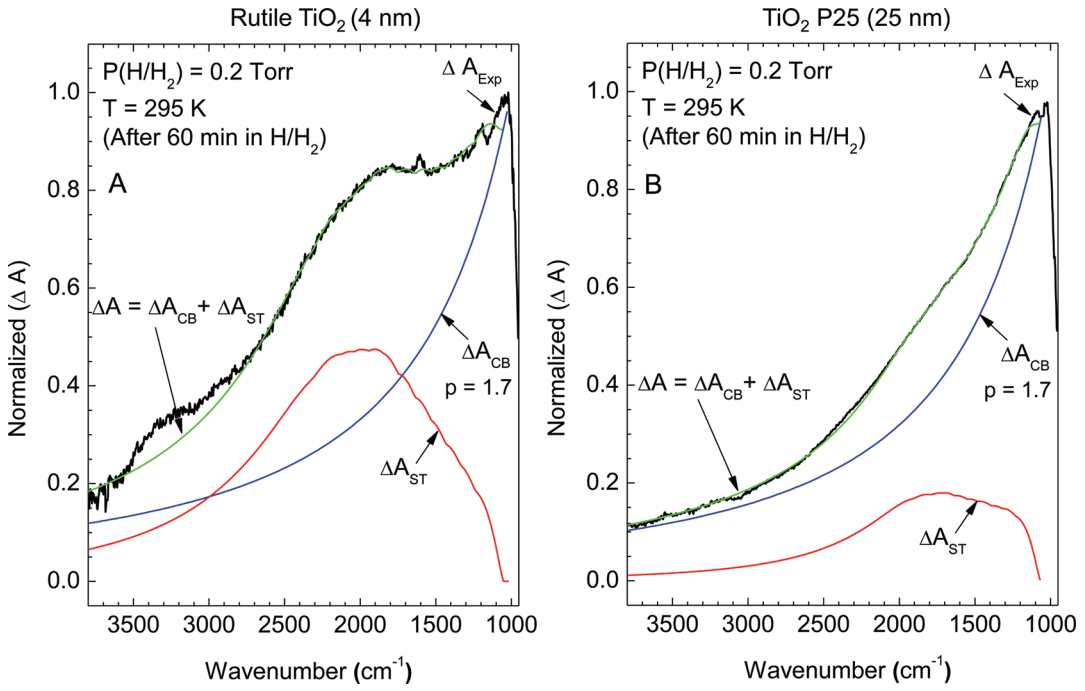

Figure 4. IR spectra of 4 nm rutile and 25 nm P25 TiO_2 particles recorded after 60 min exposure to atomic hydrogen at 295 K. As in Figure 1, the red trace is a model for the spectral response for shallow-trapped electrons and the blue line is the model for the IR spectrum of the free conduction band electrons. The direct sum of these two models is shown in green (see the text for details and fitting parameters).

suggests that this feature is of electronic origin and may be due to the STEs.

Further evidence for the electronic nature of the two broad spectral features comes from the inset in Figure 3A. The inset shows that the intensity of the broad absorbance at 1800 cm^{-1} decreases immediately upon removal of the source of UV photons. Furthermore, the broad absorbance was completely quenched upon introduction of O_2 gas, an excellent electron scavenger,[6,8,23,24] into the system.

The physical description of the electronics that emerges from Figure 3A is that UV photons, which span a large energy range, promoted electrons from the valence band of TiO_2 into the shallow-trap states within the band gap and into the conduction band. Recombination of shallow-trapped electrons and holes occurs on a very short time scale, even at 180 K, which, for clean particles, precluded observation by IR absorption (Figure 1A). However, enough delocalized conduction-band electrons survived at this temperature for detection with infrared spectroscopy. In contrast, the methanol-covered surface (Figure 3) extended the lifetime of the shallow trapped electrons by sequestering the holes. The complementary electrons to the methanol-trapped holes remained at their shallow trap sites, which are the result of morphological defects, vacancies, interstitial or impurity atoms, etc.[6,8,9] The electrons that populated these trap states were then available to absorb IR photons and become excited into the CB via direct optical transitions.[78,84,86]

The composite effects of absorption by CBEs and STEs appear as two broad, but distinct, spectral features as shown in Figure 3B. The green line in Figure 3B shows a fit to the experimental data derived by using a model based on these two components. The fit was accomplished by first using eq 1 to model the free CBEs, with a scattering constant of $p = 1.7$ (identical to the scattering constant that provided an excellent fit for the clean particles, shown in Figure 1A). As done for the clean particles, this model for the free CBE absorption (ΔA_{CB}) was fit to the experimental data in Figure 3B by matching it to the maximum at the wavenumber where the spectral cutoff begins. After modeling the purely exponential component of the signal due to CBEs, the remaining IR signal was assigned to absorption by STEs. The IR absorption of STEs (ΔA_{ST}) was modeled using eq 4, which extends eq 3 to include a weighted sum of different contributions to the optical excitation energy, E^i_{op}, which was constructed to account for broadening of the sharp donor level (E_d) that occurs for elevated concentrations of trapped electrons.[78]

$$\Delta A_{ST} = A_0 \sum_i \alpha_i \frac{(E - E^i_{op})^{3/2}}{E(E - E^i_{op} + E_{DI})^4} \quad (4)$$

In this equation, the thermal excitation energy, E_{th}, was replaced by the experimentally determined E_{DI}, as described above (Figure S2 in the Supporting Information describes implementation of this model).

The two-component model, $\Delta A = \Delta A_{CB} + \Delta A_{ST}$, provides an excellent fit to the data, ΔA_{Exp}, and appears to accurately describe the electronic character of the UV-exposed rutile particles. The parameters that provide the best fit to the data, as shown by the green line in Figure 3B, are $E_{DI} = 0.06$ eV and E^i_{op} ranging from 0.12 to 0.3 eV. When the concentration of trapped electrons is sufficiently high, the sharp donor level (E_d) can be transformed into a band.[78] That is, Coulombic interactions between the electrons can form a Hubbard gap with an occupied lower sub-band and an empty upper band.[78] According to the hydrogenic model for defect states, the Hubbard gap is similar to E_d and the upper Hubbard sub-band overlaps with the conduction band.[78] Thus, the UV-irradiation of methanol-covered rutile particles produces shallow donor levels that are 0.12−0.3 eV below the CBM, i.e., a narrow bandwidth of only ~0.18 eV. This range of excitation energies

dx.doi.org/10.1021/jp2053103 | J. Phys. Chem. C 2012, 116, 4535−4544

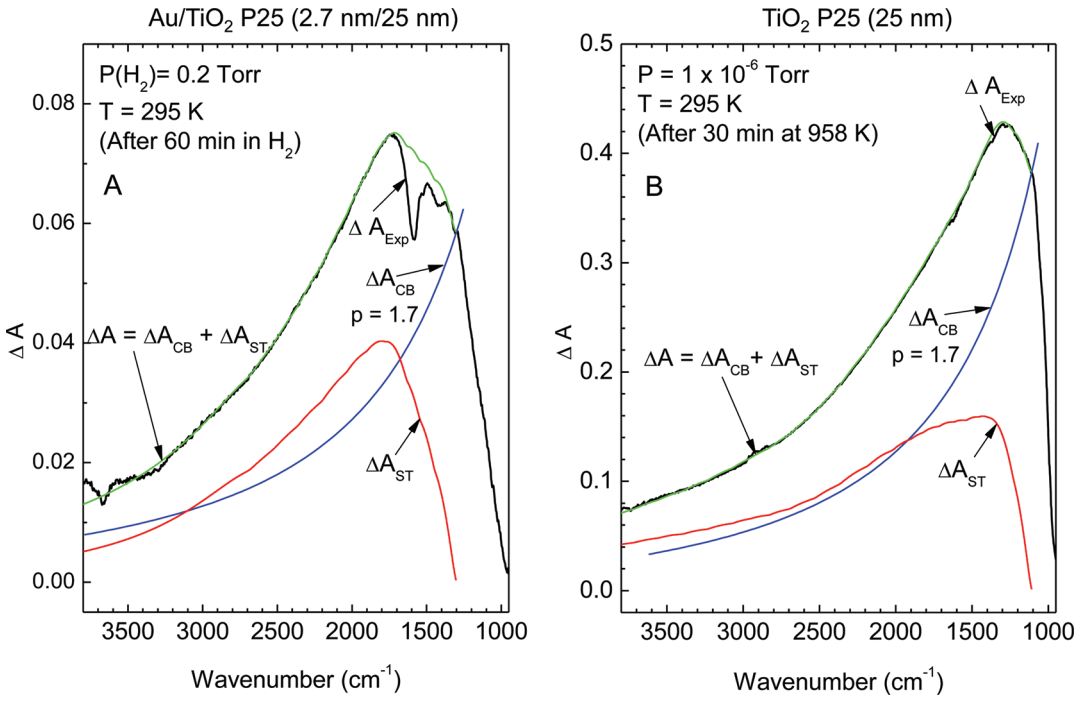

Figure 5. Panel A: IR spectrum of the Au/TiO_2 sample after 60 min exposure to molecular H_2. Panel B: IR spectrum of the P25 TiO_2 sample at 295 K that was previously reduced by heating to 958 K under high vacuum (1×10^{-6} Torr) for 30 min. As in Figure 1, the red trace is a model for the spectral response for shallow-trapped electrons and the blue line is the model for the IR spectrum of the free conduction band electrons. The direct sum of these two models is shown in green (see the text for details and fitting parameters).

is close to the experimental values reported for the energies of donor-defect states in single crystal (0.2,[92,93] 0.27,[28] and 0.3 eV[94]) and polycrystalline (0.3,[95] 0.32,[84] and 0.41 eV[96]) TiO_2. Baker et al.[95] recently proposed that, in TiO_2 nanoparticles, grain boundaries produce defect states located ~0.3 eV below the conduction band edge. Other scientists have assigned the shallow trap states in nanoparticulate TiO_2 to oxygen vacancies with various energies.[96] Although there remains little consensus between the theories for the origin of shallow trap states in TiO_2,[29,31,37,38,49,86] the two-component model described here may help guide future research efforts in this area.

3.4. Free CB and ST Electrons in Atomic Hydrogen n-Doped TiO_2 Nanoparticles. In addition to accurately describing the electronic response of titania to UV excitation, the two-component model can also be employed to develop an understanding of the infrared spectra for titania that arises from alternate methods of generating conduction band and shallow trapped electrons. For example, previous studies have suggested that H atoms effectively donate an electron to host particles to create polaron-like[58] defects, thereby populating both shallow trapped and conduction band states.[58] Theoretical work based on DFT methods have shown that hydrogen can form shallow donor levels in a number of different oxides, including TiO_2[97,98] and ZnO.[97−99] Recent DFT+U and hybrid functional studies by Di Valentin et al.[29] reported four different types of Ti^{3+} centers that are associated with donor states in the band gap of bulk anatase. In particular, their work indicates that Ti_{6c}^{3+}−OH moieties associated with H atom doping exist 0.4 eV below the conduction band.[29] Experimentally, IR transitions due to absorption by free CB electrons have been observed for H atom n-doped TiO_2[58] and ZnO[100] as well as for ZnO reduced in an H_2 atmosphere at high temperature.[75] In their work, the authors of refs 57 and 58 further suggest that the observation of a broad component to the infrared spectra for H atom n-doped TiO_2 is related to STE transitions. We have explored these effects by exposing the nanoparticulate TiO_2 samples, described above, to atomic hydrogen.

Figure 4A,B shows IR spectra recorded for both 4 nm rutile and 25 nm P25 TiO_2 upon exposure to atomic hydrogen. These experiments were performed in the dark. Our measurements demonstrate that population of electronic states upon n-doping titania particles results in IR spectra that are nearly identical to the spectra resulting from UV photoexcitation. The green lines in Figure 4A,B represent fits to the observed spectra by the two-component model for CBEs (eq 1) and STEs (eq 4) described above. Interestingly, we found that the larger particulate P25 TiO_2 sample, with a predominant phase of anatase (80 wt % anatase and 20 wt % rutile), exhibited a much less pronounced IR absorption due to STEs. Specifically, only 20% of the total absorbance signal in Figure 4 can be attributed to STEs for the n-doped P25 sample (~25 nm), as compared to 45% for 4 nm rutile particles. This observation likely reflects the varying ability of the two TiO_2 polymorphs to stabilize a redox change; i.e., the two polymorphs differ in their propensities for charge trapping and transfer at their surfaces.[9] For example, Komaguchi et al.[101] found that rutile is more easily reduced with H_2 or during vacuum annealing than anatase (irrespective of whether it exists as a pure phase or in the mixed-phase P25 material). In addition, the relative stability of reduced anatase and rutile as a function of particle size and degree of hydroxylation was examined theoretically by Barnard and Zapol using DFT.[102] The key discovery in their work is that, for both TiO_2 polymorphs, the ability to accommodate reduction increases as the particle size decrease below ~10 nm. The results presented in Figure 4 agree very well with these theoretical predictions. Specifically, the small, 4 nm rutile nanoparticles are found to stabilize donor-defect states (as

dx.doi.org/10.1021/jp2053103 | J. Phys. Chem. C 2012, 116, 4535−4544

reflected by the large IR signal for ST electrons) much more effectively than the 25 nm mixed-phase P25 TiO_2.

Our results are also consistent with previously proposed explanations for the high photocatalitic activity of mixed phase P25 TiO_2, which suggest that the coexistence of small amorphous particles and large crystallites facilitates charge transfer and separation.[22,103]

Beyond direct H atom n-doping of titania, we also find that the two-component model can be used to describe the IR data for TiO_2-supported Au nanoparticles that are exposed to molecular hydrogen. Hydrogen molecules are known to dissociate on the surface of TiO_2-supported Au nanoparticles.[57,104] Following dissociation, the H atoms can spill over onto the TiO_2 surface where they are expected to donate an electron to the particles to effectively n-dope the semiconductor.[57] Figure 5 A shows the IR spectrum for the H_2-exposed Au/TiO_2 sample. The IR spectrum for molecular H_2 exposed to pure TiO_2 particles (not shown) does not exhibit features above the baseline. Figure 4 shows that the presence of Au nanoparticles on the surface of TiO_2 led to a spectral response very similar to that for the H atom exposed samples.

3.5. Free CB and ST Electrons in Thermally Annealed TiO_2 Nanoparticles. In addition to intentionally n-doping the titania samples, another well-known method of creating excess electrons is to remove lattice oxygen by thermal treatment above 670 K in vacuum.[61,105] Therefore, we have studied the infrared response of a P25 TiO_2 sample that was held at 958 K under high vacuum (1×10^{-6} Torr) for 30 min. Following the annealing step and cooling the sample to room temperature, we found that the new IR signal due to electronic transitions persisted for several hours. The resulting spectrum is shown in Figure 5B. As for the UV-exposed TiO_2, the IR signal quickly returned to baseline upon the introduction of an electron scavenger.[61,105,106] The model shown by the green line in Figure 5B reveals that this IR electronic absorption is most likely due to both CBEs and STEs. The optical depth of the shallow donor levels created by removal of lattice oxygen, i.e., by creation of O_{vac} sites, is about the same (0.14−0.26 eV) as that produced by n-doping the Au/TiO_2 P25 and pure P25 TiO_2 samples.

3.6. Relation to Previous Work. Above, we presented three different approaches for populating excited electronic states in TiO_2: UV-irradiation in the presence of a hole scavenger, n-doping by atomic hydrogen, and thermal removal of lattice oxygen. The infrared spectra recorded for the excited titania particles all exhibit two distinct contributions: (1) a featureless IR absorbance that rises exponentially with wavelength according to eq 1, spanning the range 4000−1000 cm^{-1}, and (2) a broad feature that peaks at 1800 cm^{-1} that can be modeled by eq 4, which includes a range of optical transition energies. The ability of these two models to accurately describe the data strongly suggests that the first component to the IR data is due to absorption by delocalized electrons in the conduction band and that electrons localized at donor states that exist just below the conduction band edge are responsible for the latter infrared feature. In the case of CBEs, acoustic phonons are required to couple to the delocalized electrons in order for an IR-allowed transition to occur. The STEs are excited by the IR photons through direct absorption, as described by a hydrogenic-effective mass model.

Previous experimental studies have also demonstrated that infrared spectroscopy can be used to probe electronic excitations within TiO_2. Of particular relevance to the work described above, Yamakata et al. hypothesized that their infrared absorbance signal for photoexcited TiO_2 originated from electrons trapped in shallow midgap states via two routes: intraconduction band transitions of free electrons that had been thermally excited from the trap state and direct optical transitions from the trap state to the conduction band.[64] However, these two contributions were not resolved in their room temperature experiments, likely due to rapid recombination of the shallow-trapped electrons.[57,58] In addition, UV-photoexcitation of TiO_2 in the presence of a hole scavenger has previously been shown to produce featureless mid-IR absorption due to free CB electrons[62,66] and visible range absorption due to electrons trapped at energy levels deeper than 1 eV below the conduction band minimum.[45,49]

Recently, Mattioli et al., using LSD-GGA+U *ab initio* simulations, explored the nature of both deeply trapped and conduction-band electrons in reduced TiO_2.[38] They have shown that O_{vac} and Ti_{int} defects exhibit polaron behavior, with charge localization at Ti^{3+} sites and that appreciable structural rearrangement occurs upon their formation, in both rutile and anatase. These studies predict that the defects give rise to vertical transition levels about 1 eV below the CBM and to thermodynamic transition levels much closer to the CB edge. The emerging understanding from their work appears to be that O_{vac} and Ti_{int} defects may play a role as deep donors prior to significant structural relaxations and as shallow donors when structural relaxation occurs. Further supporting these conclusions, are the studies by Bogomolov et al.[89] and Deskins et al.,[49] which show that electronic conductivity in TiO_2 is due to the formation of a small polaron with a hopping energy of ~0.13 eV. It appears that the excess electrons in n-doped TiO_2 spend the majority of time trapped at Ti sites and that the electronic motion to neighboring Ti sites is mediated by the CB. These theoretical descriptions of the electronic nature of n-doped TiO_2 are strongly supported by the experimental observations reported here, which show strong evidence for both delocalized CBEs and localized STEs that are in thermodynamic equilibrium with one another. The energy of donor-defect states defined in this work, 0.12−0.3 eV below the CB edge, agree well with the previously reported values for single crystal (0.2,[92,93] 0.27,[28] and 0.3 eV[94]) and for polycrystalline (0.3,[95] 0.32,[84] and 0.41 eV[96]) TiO_2.

4. CONCLUSION

In this work, we have shown experimental evidence that supports the emerging description of the electronic structure of n-doped and photoexcited TiO_2, which is governed by defects that serve as electron donor levels within the band gap of the semiconductor. Both localized (below the CBM) and delocalized (within the CB) electrons exist in TiO_2 when excess electrons (defects) are created. We have demonstrated that IR radiation can excite the fraction of electrons that are trapped at shallow donor levels 0.12−0.3 eV below the CBM into the CB. These band-to-band transitions are evidenced by a broad IR absorption with a maximum characteristic of the donor level energy. In addition, free CBEs are detected via infrared spectroscopy. The CBEs exhibit a broad featureless absorbance that increases exponentially across the entire mid-IR range. Together, these experimental observations provide new insight into the electronic structure of titania nanoparticles and demonstrate the utility of transmission FTIR for probing electronic transitions within semiconductor materials.

dx.doi.org/10.1021/jp2053103 | J. Phys. Chem. C 2012, 116, 4535−4544

■ ASSOCIATED CONTENT

Supporting Information

Figures S1 and S2. This material is available free of charge via the Internet at http://pubs.acs.org.

■ AUTHOR INFORMATION

Corresponding Author

*Tel: (540) 231-2472; e-mail: jrmorris@vt.edu.

■ ACKNOWLEDGMENTS

This work was supported by the Army Research Office, W911NF-09-1-0150, and the Defense Threat Reduction Agency, W911NF-06-1-0111. Professor John T. Yates Jr. is gratefully acknowledged for several helpful discussions. We thank Professor Brian M. Tissue for many helpful discussions and use of the laser-evaporation nanoparticle synthesis apparatus developed by his research group.

■ REFERENCES

(1) Diebold, U. *Surf. Sci. Rep.* **2003**, *48*, 53.
(2) Pang, C. L.; Lindsay, R.; Thornton, G. *Chem. Soc. Rev.* **2008**, *37*, 2328.
(3) Hoffmann, M. R.; Martin, S. T.; Choi, W. Y.; Bahnemann, D. W. *Chem. Rev.* **1995**, *95*, 69.
(4) Carp, O.; Huisman, C. L.; Reller, A. *Prog. Solid State Chem.* **2004**, *32*, 33.
(5) Fujishima, A.; Zhang, X.; Tryk, D. A. *Surf. Sci. Rep.* **2008**, *63*, 515.
(6) Linsebigler, A. L.; Lu, G. Q.; Yates, J. T. Jr. *Chem. Rev.* **1995**, *95*, 735.
(7) Grätzel, M. *Nature* **2001**, *414*, 338.
(8) Thompson, T. L.; Yates, J. T. Jr. *Chem. Rev.* **2006**, *106*, 4428.
(9) Henderson, M. A. *Surf. Sci. Rep.* **2011**, *66*, 185.
(10) Campbell, C. T. *Surf. Sci. Rep.* **1997**, *27*, 1.
(11) Henrich, V. E.; Dresselhaus, G.; Zeiger, H. J. *Phys. Rev. Lett.* **1976**, *36*, 1335.
(12) Fox, M. A.; Dulay, M. T. *Chem. Rev.* **1993**, *93*, 341.
(13) Cronemeyer, D. C. *Phys. Rev.* **1959**, *113*, 1222.
(14) Henrich, V. E.; Dresselhaus, G.; Zeiger, H. J. *Bull. Am. Phys. Soc.* **1976**, *21*, 940.
(15) Orendorz, A.; Wüsten, J.; Ziegler, C.; Gnaser, H. *Appl. Surf. Sci.* **2005**, *252*, 85.
(16) Krischok, S.; Günster, J.; Goodman, D. W.; Höfft, O.; Kempter, V. *Surf. Interface Anal.* **2005**, *37*, 77.
(17) Wendt, S.; Sprunger, P. T.; Lira, E.; Madsen, G. K. H.; Li, Z.; Hansen, J. O.; Matthiesen, J.; Blekinge-Rasmussen, A.; Laegsgaard, E.; Hammer, B.; Besenbacher, F. *Science* **2008**, *320*, 1755.
(18) Yim, C. M.; Pang, C. L.; Thornton, G. *Phys. Rev. Lett.* **2010**, *104*, 036806.
(19) Kurtz, R. L.; Stock-Bauer, R.; Madey, T. E.; Román, E.; De Segovia, J. *Surf. Sci.* **1989**, *218*, 178.
(20) Henderson, M. A.; Epling, W. S.; Peden, C. H. F.; Perkins, C. L. *J. Phys. Chem. B* **2003**, *107*, 534.
(21) Chung, Y. W.; Lo, W. J.; Somorjai, G. A. *Surf. Sci.* **1977**, *64*, 588.
(22) Hurum, D. C.; Agrios, A. G.; Gray, K. A.; Rajh, T.; Thurnauer, M. C. *J. Phys. Chem. B* **2003**, *107*, 4545.
(23) Berger, T.; Sterrer, M.; Diwald, O.; Knözinger, E.; Panayotov, D.; Thompson, T. L.; Yates, J. T. Jr. *J. Phys. Chem. B* **2005**, *109*, 6061.
(24) Berger, T.; Sterrer, M.; Diwald, O.; Knözinger, E. *ChemPhysChem* **2005**, *6*, 2104.
(25) Khomenko, V. M.; Langer, K.; Rager, H.; Fett, A. *Phys. Chem. Miner.* **1998**, *25*, 338.
(26) Hasiguti, R. R.; Yagi, E. *Phys. Rev. B* **1994**, *49*, 7251.
(27) Yagi, E.; Hasiguti, R. R.; Aono, M. *Phys. Rev. B* **1996**, *54*, 7945.
(28) Ghosh, A. K.; Wakim, F. G.; Addiss, R. R. *Phys. Rev.* **1969**, *184*, 979.
(29) Di Valentin, C.; Pacchioni, G.; Selloni, A. *J. Phys. Chem. C* **2009**, *113*, 20543.
(30) Fujimori, A.; Bocquet, A. E.; Morikawa, K.; Kobayashi, K.; Saitoh, T.; Tokura, Y.; Hase, I.; Onoda, M. *J. Phys. Chem. Solids* **1996**, *57*, 1379.
(31) Finazzi, E.; Valentin, C. D.; Pacchioni, G.; Selloni, A. *J. Chem. Phys.* **2008**, *129*, 154113.
(32) Krüger, P.; Bourgeois, S.; Domenichini, B.; Magnan, H.; Chandesris, D.; Le Févre, P.; Flank, A. M.; Jupille, J.; Floreano, L.; Cossaro, A.; Verdini, A.; Morgante, A. *Phys. Rev. Lett.* **2008**, *100*, 055501.
(33) Finazzi, E.; Di Valentin, C.; Pacchioni, G. *J. Phys. Chem. C* **2009**, *113*, 3382.
(34) Minato, T.; Sainoo, Y.; Kim, Y.; Kato, H. S.; Aika, K.-i.; Kawai, M.; Zhao, J.; Petek, H.; Huang, T.; He, W.; Wang, B.; Wang, Z.; Zhao, Y.; Yang, J.; Hou, J. G. *J. Chem. Phys.* **2009**, *130*, 124502.
(35) Brandão, F. D.; Pinheiro, M. V. B.; Ribeiro, G. M.; Medeiros-Ribeiro, G.; Krambrock, K. *Phys. Rev. B* **2009**, *80*, 235204.
(36) Papageorgiou, A. C.; Beglitis, N. S.; Pang, C. L.; Teobaldi, G.; Cabailh, G.; Chen, Q.; Fisher, A. J.; Hofer, W. A.; Thornton, G. *Proc. Natl. Acad. Sci. U. S. A.* **2010**, *107*, 2391.
(37) Janotti, A.; Varley, J. B.; Rinke, P.; Umezawa, N.; Kresse, G.; Van de Walle, C. G. *Phys. Rev. B* **2010**, *81*, 085212.
(38) Mattioli, G.; Alippi, P.; Filippone, F.; Caminiti, R.; Amore Bonapasta, A. *J. Phys. Chem. C* **2010**, *114*, 21694.
(39) Ganduglia-Pirovano, M. V.; Hofmann, A.; Sauer, J. *Surf. Sci. Rep.* **2007**, *62*, 219.
(40) Dohnálek, Z.; Lyubinetsky, I.; Rousseau, R. *Prog. Surf. Sci.* **2010**, *85*, 161.
(41) Yim, C. M.; Pang, C. L.; Thornton, G. *Phys. Rev. Lett.* **2010**, *104*, 259704.
(42) Wendt, S.; Bechstein, R.; Porsgaard, S.; Lira, E.; Hansen, J. Ø.; Huo, P.; Li, Z.; Hammer, B.; Besenbacher, F. *Phys. Rev. Lett.* **2010**, *104*, 259703.
(43) Zhang, Z.; Lee, J.; Yates, J. T.; Bechstein, R.; Lira, E.; Hansen, J. Ø.; Wendt, S.; Besenbacher, F. *J. Phys. Chem. C* **2010**, *114*, 3059.
(44) Di Valentin, C.; Pacchioni, G.; Selloni, A. *Phys. Rev. Lett.* **2006**, *97*, 166803.
(45) Kowalski, P. M.; Camellone, M. F.; Nair, N. N.; Meyer, B.; Marx, D. *Phys. Rev. Lett.* **2010**, *105*, 146405.
(46) Lambrecht, W. R. L. *Phys. Status Solidi B* **2010**, 1.
(47) Wang, Z.-W.; Shu, D.-J.; Wang, M.; Ming, N.-B. *Phys. Rev. B* **2010**, *82*, 165309.
(48) Mattioli, G.; Filippone, F.; Alippi, P.; Bonapasta, A. A. *Phys. Rev. B* **2008**, *78*, 241201.
(49) Deskins, N. A.; Rousseau, R.; Dupuis, M. *J. Phys. Chem. C* **2009**, *113*, 14583.
(50) Stausholm-Møller, J.; Kristoffersen, H. H.; Hinnemann, B.; Madsen, G. K. H.; Hammer, B. *J. Chem. Phys.* **2010**, *133*, 144708.
(51) Mulheran, P. A.; Nolan, M.; Browne, C. S.; Basham, M.; Sanville, E.; Bennett, R. A. *Phys. Chem. Chem. Phys.* **2010**, *12*, 9763.
(52) Chiodo, L.; García-Lastra, J. M.; Iacomino, A.; Ossicini, S.; Zhao, J.; Petek, H.; Rubio, A. *Phys. Rev. B* **2010**, *82*, 045207.
(53) Kang, W.; Hybertsen, M. S. *Phys. Rev. B* **2010**, *82*, 085203.
(54) Panayotov, D. A.; Burrows, S.; Mihaylov, M.; Hadjiivanov, K.; Tissue, B. M.; Morris, J. R. *Langmuir* **2010**, *26*, 8106.
(55) In *Highly Dispersed Metallic Oxides Produced by Aerosil Process. Degussa Technical Bulletin Pigments*; Degussa AG: Frankfurt, Germany, 1990; Vol. *56*, p 13.
(56) Addamo, M.; Augugliaro, V.; Di Paola, A.; Garcia-Lopez, E.; Loddo, V.; Marci, G.; Molinari, R.; Palmisano, L.; Schiavello, M. *J. Phys. Chem. B* **2004**, *108*, 3303.
(57) Panayotov, D. A.; Yates, J. T. Jr. *J. Phys. Chem. C* **2007**, *111*, 2959.
(58) Panayotov, D. A.; Yates, J. T. Jr. *Chem. Phys. Lett.* **2007**, *436*, 204.
(59) Thompson, T. L.; Panayotov, D. A.; Yates, J. T. Jr. *J. Phys. Chem. B* **2004**, *108*, 16825.
(60) Zhang, H.; Banfield, J. F. *J. Mater. Res.* **2000**, *15*, 437.

(61) Panayotov, D. A.; Yates, J. T. Jr. *Chem. Phys. Lett.* **2005**, *410*, 11.
(62) Zhao, H.; Zhang, Q.; Weng, Y.-X. *J. Phys. Chem. C* **2007**, *111*, 3762.
(63) Tamaki, Y.; Hara, K.; Katoh, R.; Tachiya, M.; Furube, A. *J. Phys. Chem. C* **2009**, *113*, 11741.
(64) Yamakata, A.; Ishibashi, T.-a.; Onishi, H. *Chem. Phys. Lett.* **2001**, *333*, 271.
(65) Yamakata, A.; Ishibashi, T.; Onishi, H. *J. Phys. Chem. B* **2002**, *106*, 9122.
(66) Yoshihara, T.; Katoh, R.; Furube, A.; Tamaki, Y.; Murai, M.; Hara, K.; Murata, S.; Arakawa, H.; Tachiya, M. *J. Phys. Chem. B* **2004**, *108*, 3817.
(67) Baraton, M.-I.; Merhari, L. *Scr. Mater.* **2001**, *44*, 1643.
(68) Szczepankiewicz, S. H.; Colussi, A. J.; Hoffmann, M. R. *J. Phys. Chem. B* **2000**, *104*, 9842.
(69) Yamakata, A.; Ishibashi, T.; Onishi, H. *J. Phys. Chem. B* **2001**, *105*, 7258.
(70) Warren, D. S.; McQuillan, A. J. *J. Phys. Chem. B* **2004**, *108*, 19373.
(71) Hao, E.; Anderson, N. A.; Asbury, J. B.; Lian, T. *J. Phys. Chem. B* **2002**, *106*, 10191.
(72) Chen, T.; Wu, G.-p.; Feng, Z.-c.; Shi, J.-y.; Ma, G.-j.; Ying, P.-l.; Li, C. *Chin. J. Chem. Phys.* **2007**, 483.
(73) Davydov, A. *Molecular Spectroscopy of Oxide Catalyst Surfaces*; John Wiley & Sons: Chichester, 2003.
(74) Harrick, N. J. *J. Phys. Chem. Solids* **1960**, *14*, 60.
(75) McCluskey, M. D.; Jokela, S. J.; Zhuravlev, K. K.; Simpson, P. J.; Lynn, K. G. *Appl. Phys. Lett.* **2002**, *81*, 3807.
(76) Smith, R. A. *Semiconductors*; Cambridge University Press: Cambridge, UK, 1978.
(77) Pankove, J. I. *Optical Processes in Semiconductors*; Dover: New York, 1975.
(78) Cox, P. A. *Transition Metal Oxides: an Introduction to their Electronic Structure and Properties*; Clarendon Press: Oxford, 1992.
(79) Thompson, T. L.; Panayotov, D. A.; Yates, J. T. Jr.; Martyanov, I.; Klabunde, K. J. *J. Phys. Chem. B* **2004**, *108*, 17857.
(80) Szczepankiewicz, S. H.; Moss, J. A.; Hoffmann, M. R. *J. Phys. Chem. B* **2002**, *106*, 2922.
(81) Landau, L. D. *Phys. Z. Sowjetunion* **1933**, *3*, 664.
(82) Mott, N. F.; Gurney, R. W. *Electronic Processes in Ionic Crystals*; Oxford University Press: London, 1940.
(83) Brus, L. *J. Phys. Chem.* **1986**, *90*, 2555.
(84) Weng, Y.-X.; Wang, Y.-Q.; Asbury, J. B.; Ghosh, H. N.; Lian, T. *J. Phys. Chem. B* **1999**, *104*, 93.
(85) Kukimoto, H.; Shionoya, S.; Koda, T.; Hioki, R. *J. Phys. Chem. Solids* **1968**, *29*, 935.
(86) Austin, I. G.; Mott, N. F. *Adv. Phys.* **2001**, *50*, 757.
(87) Kukimoto, H.; Hioki, R.; Koda, T.; Shionoya, S. *Phys. Lett.* **1965**, *19*, 551.
(88) Austin, I. G.; Mott, N. F. *Adv. Phys.* **1969**, *18*, 41.
(89) Bogomolov, V. N.; Kudinov, E. K.; Mirlin, D. N.; Firsov, Y. A. *Sov. Phys. Solid State* **1968**, *9*, 1630.
(90) Tamaki, Y.; Furube, A.; Murai, M.; Hara, K.; Katoh, R.; Tachiya, M. *J. Am. Chem. Soc.* **2006**, *128*, 416.
(91) Thompson, T. L.; Yates, J. T. Jr. *J. Phys. Chem. B* **2005**, *109*, 18230.
(92) Bogomolov, V. N.; Mirlin, D. N. *Phys. Status Solidi* **1968**, *27*, 443.
(93) Haiffe, K.; Hupfeld, J.; Wetterling, J. *Z. Phys. Chem. (Munich)* **1976**, *103*, 115.
(94) Fan, F. R. F.; Bard, A. J. *J. Phys. Chem.* **1990**, *94*, 3761.
(95) Baker, L. R.; Hervier, A.; Seo, H.; Kennedy, G.; Komvopoulos, K.; Somorjai, G. A. *J. Phys. Chem. C* **2011**, *115*, 16006.
(96) Serpone, N.; Lawless, D.; Khairutdinov, R. *J. Phys. Chem.* **1995**, *99*, 16646.
(97) Kilic, C.; Zunger, A. *Appl. Phys. Lett.* **2002**, *81*, 73.
(98) Robertson, J.; Peacock, P. W. *Thin Solid Films* **2003**, *445*, 155.
(99) Van de Walle, C. G.; Neugebauer, J. *Nature* **2003**, *423*, 626.
(100) Noei, H.; Qiu, H.; Wang, Y.; Muhler, M.; Wöll, C. *ChemPhysChem* **2010**, *11*, 3604.
(101) Komaguchi, K.; Nakano, H.; Araki, A.; Harima, Y. *Chem. Phys. Lett.* **2006**, *428*, 338.
(102) Barnard, A. S.; Zapol, P. *Phys. Rev. B* **2004**, *70*, 235403.
(103) Bickley, R. I.; Gonzalez-Carreno, T.; Lees, J. S.; Palmisano, L.; Tilley, R. J. D. *J. Solid State Chem.* **1991**, *92*, 178.
(104) Boronat, M.; Concepción, P.; Corma, A. *J. Phys. Chem. C* **2009**, *113*, 16772.
(105) Panayotov, D.; Yates, J. T. Jr. *Chem. Phys. Lett.* **2003**, *381*, 154.
(106) Panayotov, D. A.; Yates, J. T. Jr. *Chem. Phys. Lett.* **2004**, *399*, 300.